Accelerating *ab initio* calculation of phonon dispersion curves: q-point convergence

Katalin Gaál-Nagy*

Institut für Theoretische Physik, Universität Regensburg, D-93040 Regensburg, Germany and European Theoretical Spectroscopy Facility (ETSF), CNISM-CNR-INFM, and Dipartimento di Fisica, dell'Università degli Studi di Milano, via Celoria 16, I-20133 Milano, Italy

(Received 12 September 2007; published 23 January 2008)

I present a scheme for describing the long-range interatomic force constants, which is more accurate than the procedure which is commonly used within plane-wave based density-functional perturbation-theory calculations. The scheme is based on the inclusion of a **q**-point grid which is denser in a restricted region around the center of the Brillouin zone than in the remaining parts, although the scheme is applicable to other regions. I have tested the validity of the procedure in the case of high-pressure body-centered tetragonal and simple hexagonal phases of bulk silicon.

DOI: 10.1103/PhysRevB.77.024309 PACS number(s): 61.50.Ks, 63.20.D−, 71.15.Nc

I. INTRODUCTION

The calculation of vibrational properties of solids, surfaces, and nanocrystals plays an important role in the structural characterization of matter. Besides the possibility to compare the vibrational frequencies with experimental data, phonon modes can also be used to determine the structural stability of a system.[1–5] This requires a reliable description of the vibrational properties of a system. Nowadays, *ab initio* methods based on the density-functional perturbation theory (DFPT)[6] or frozen-phonon techniques[7] are commonly used for this purpose. With the latter, the phonon frequencies can be obtained by calculating the dynamical matrix for each **q** point along the high-symmetry directions of the Brillouin zone (BZ), which can be quite cumbersome. In the former case, the dynamical matrices are computed just on a (finite) grid of **q** points in the irreducible wedge of the Brillouin zone (IBZ) with subsequent Fourier interpolation. Because of the computational effort of these calculations, the grid is often taken as coarse as possible resulting sometimes in an inaccurate description of the long-range force constants yielding erroneous frequencies, especially in the low-frequency range near the Γ point. However, inaccurate force constants can result in wrong frequencies everywhere in the Brillouin zone.

Considering the investigation of the thermodynamic stability of the system, an error in the description of the low-frequency area close to Γ, the center of the BZ, plays just a minor role for the calculation of the free energy. However, for the investigation of the Grüneisen parameters or the thermal expansion especially at low temperatures, it is particularly necessary to describe these frequencies correctly, since their reciprocal value enters the formula.[8] Furthermore, if someone is interested in the determination of soft phonon modes, which point at the instability of the structure, an exact description of the corresponding frequencies is necessary. A wrong description of the long-range force constants may yield imaginary frequencies for a genuinely stable structure, which are then interpreted as a result of a structural instability.

A possibility to overcome this problem has been given by Gonze and Lee[9] who corrected the long-range dipole-dipole interaction contribution to the force constants using a term which yields the correct nonanalytical behavior in the limit of small $|\mathbf{q}|$ similar to the nonanalytic corrections yielding the LO-TO splitting. With this procedure, the description of phonons close to Γ is significantly improved, and the required number of **q** points is reduced. However, this scheme was demonstrated only for semiconductors, and the possibility to employ it in the case of discrepancies at points close to the boundary of the BZ has not been proven yet.

I have taken another approach to overcome the problem of the correct description of the long-range force constants within DFPT, which is related to the **q**-point convergence by introducing a mini-Brillouin zone (mini-BZ). Inside of this mini-BZ, the dynamical matrices are computed for a denser mesh of **q** points. The mini-BZ can be chosen not only around the center of the BZ but also at its boundary. These additional contributions are taken into account in the determination of the force constants. The validity of this procedure has been verified in the case of the high-pressure phases of bulk silicon: I have chosen the metallic β-tin body-centered tetragonal (bct) and simple-hexagonal (sh) phases. In both cases, structures at volumes beyond the range of structural stability of the phase have been selected. The method yields an improved description of the phonon dispersion curves using less **q** points than the standard refinement of the grid. In detail, imaginary frequencies for the bct structure near Γ from standard procedure have been traced back to erroneous force constants, whereas the soft phonon mode for the sh structure has been verified.

This paper is organized as follows. In Sec. II, I describe the theoretical framework of the method and in Sec. III, the way of application. Next, a short review of the technical details of the investigation is given (Sec. IV). In Sec. V, I apply the procedure to the bct (Sec. V A) and the sh (Sec. V B) structures of bulk silicon, where the results are compared and discussed afterwards in Sec. V C. Finally, I summarize and draw a conclusion (Sec. VI).

II. THEORY

In general, the phonon frequencies $\omega_j(\mathbf{q})$ at a given **q** point in the BZ are obtained by diagonalizing the dynamical matrix $\mathbf{D}_{\alpha\alpha'}(\kappa\kappa',\mathbf{q})$, i.e., by solving the equation

$$\|\mathbf{D}_{\alpha\alpha'}(\kappa\kappa',\mathbf{q}) - \omega^2(\mathbf{q})\mathbf{1}_{3N_A}\| = 0, \tag{1}$$

where κ, κ' label the sublattices (the basis atoms), α,α' are the Cartesian coordinates, and $\mathbf{1}_{3N_A}$ is the $3N_A \times 3N_A$ unitary matrix for N_A atoms in the cell. I focus on the Fourier-interpolation scheme to obtain the frequencies along the high-symmetry directions of the BZ. To this end, DFPT calculations of the dynamical matrices are performed for $\mathbf{q}$ points on a finite, regular grid. These dynamical matrices are connected with the force constant matrices $\Phi_{\alpha\alpha'}\binom{l\ l'}{\kappa\ \kappa'}$ by a discrete Fourier transform (FT),

$$\mathbf{D}_{\alpha\alpha'}(\kappa\kappa',\mathbf{q}) = \sum_{ll'} \Phi_{\alpha\alpha'}\begin{pmatrix} l & l' \\ \kappa & \kappa' \end{pmatrix} \exp\left\{ -i\mathbf{q}\cdot\left[\mathbf{R}\begin{pmatrix} l \\ \kappa \end{pmatrix} - \mathbf{R}\begin{pmatrix} l' \\ \kappa' \end{pmatrix}\right]\right\}, \tag{2}$$

where $\mathbf{R}(l,\kappa)$ is the coordinate of the κth atom in the lth cell. Using the common procedure within plane-wave codes, one calculates the force constants by an FT from the dynamical matrices for the $\mathbf{q}$ points from the discrete and finite grid and subsequently obtains the dynamical matrices for any $\mathbf{q}$ point by FT of the force constant matrices. However, the drawback of this procedure is that the range of the forces is related to the choice of the $\mathbf{q}$ points: an $l_1 \times l_2 \times l_3$ grid of $\mathbf{q}$ points leads to the inclusion of interatomic force constants between atoms within $l_1 \times l_2 \times l_3$ cells. In other words, assuming a finer $\mathbf{q}$-point grid, one can extend the range of the forces included in the force constants. Convergence tests usually have to be performed by comparing the phonon dispersion curves for calculations based on various grids. However, the number of $\mathbf{q}$ points is $l_1 \times l_2 \times l_3$ in the BZ (which can be reduced by symmetry), and therefore, most investigations are restricted to a smaller set of $\mathbf{q}$ points with a less accurate description of the long-range force constants.

The long-range force constants particularly affect the low-frequency phonons close to the Γ point which might be wrongly described within this procedure. This problem can be overcome for semiconductors by using the method described in Ref. 9 or by using more $\mathbf{q}$ points to sample the BZ. Another possibility is to use more $\mathbf{q}$ points only in the area close to Γ which I have chosen here. In particular, I have taken a denser grid just in a small area around Γ (mini-BZ), and I assume a less dense grid outside this mini-BZ. Since the FT is based on a regular grid, I interpolate the missing dynamical matrices outside the mini-BZ by an FT from the force constants based on the coarser grid. In the following description, I neglect the indices κ and α for simplicity, and I investigate the case $l_1 = l_2 = l_3$ only. The case $l_1 \neq l_2 \neq l_3$ follows analogously.

Assuming a $n \times n \times n$ grid, the force constants Φ^{nnn} are obtained by FT from the corresponding dynamical matrices $\mathbf{D}^{nnn}$ calculated within DFPT,

$$\mathbf{D}^{nnn}(\mathbf{q}) \xrightarrow{\text{FT}} \Phi^{nnn}. \tag{3}$$

From these force constants Φ^{nnn}, the dynamical matrices for any $\mathbf{q}$ point in the BZ can be calculated by a back FT, therefore, also for the $\mathbf{q}$ points on a finer grid, e.g., on an $l \times l \times l$ grid with $l > n$. Thus, one gets

$$\Phi^{nnn} \xrightarrow{\text{FT}} \mathbf{D}^{lll}_{\text{int}}(\mathbf{q}), \tag{4}$$

and from these dynamical matrices $\mathbf{D}^{lll}_{\text{int}}(\mathbf{q})$, one can also get again force constants $\tilde{\Phi}^{lll}_{\text{int}}$ by

$$\mathbf{D}^{lll}_{\text{int}}(\mathbf{q}) \xrightarrow{\text{FT}} \tilde{\Phi}^{lll}_{\text{int}}, \tag{5}$$

which are in this case identical to Φ^{nnn}. In a next step I have performed calculations of the dynamical matrices $\mathbf{D}^{lll}(\mathbf{q} \in \text{mini-BZ})$ for $\mathbf{q}$ points of the $l \times l \times l$ grid inside the mini-BZ using the DFPT procedure. Taking these dynamical matrices and the interpolated ones outside the mini-BZ, the improved force constants Φ^{lll}_{int} can be calculated by

$$\mathbf{D}^{lll}(\mathbf{q} \in \text{mini-BZ}) \vee \mathbf{D}^{lll}_{\text{int}}(\mathbf{q} \notin \text{mini-BZ}) \xrightarrow{\text{FT}} \Phi^{lll}_{\text{int}}. \tag{6}$$

From these force constants Φ^{lll}_{int}, the dynamical matrices for any $\mathbf{q}$, in particular along the high-symmetry directions of the BZ, are calculated in the standard way. In the limit of very fine grids, one should achieve the same results as within the procedure of Gonze and Lee.[9] However, this method is not restricted to a mini-BZ around the Γ point since the mini-BZ can be chosen arbitrarily. This has the advantage that also ranges of the dispersion curves far away from the Γ point can be improved. Besides, the shape of the phonon density of states for particular spectral features can be inspected in detail.

III. APPLICATION

In order to apply this scheme, I have modified a postprocessing routine of the QUANTUM ESPRESSO package[10] in order to write out not only the frequencies but also the complete dynamical matrices after the FT. I have checked the numerical stability of the method by comparing the phonon dispersion curves based on the force constants Φ^{888} from Eq. (3) and $\tilde{\Phi}^{888}_{\text{int}}$ from Eq. (5), and I have found differences in the frequencies of less than 0.25 cm^{-1}.

The computational gain by applying the method described in the previous section depends on the choice of the mini-BZ. Here, I want to describe a possible scheme for the determination of its extent. The mini-BZ should be chosen in a way that it covers the regions where the phonon dispersion curve is not at convergence with respect to the $\mathbf{q}$ points. Thus, one has to inspect the frequencies at some test $\mathbf{q}$ points calculated within DFPT (ω^{DFPT}) and compare them with the interpolated ones (ω^{int}). One should be aware that the test $\mathbf{q}$ points are not equal to the grid points used for the interpolated curves. In principle, these test $\mathbf{q}$ points can be chosen arbitrarily, but it is useful to choose them as grid points of the next finer grid; e.g., if the phonon dispersion curves have been calculated on a $n \times n \times n$ grid, the test $\mathbf{q}$ points should be $2n \times 2n \times 2n$ grid points. Note that going from a $n \times n \times n$ grid to a $2n \times 2n \times 2n$ one, the range of the force constants is doubled. This choice is justified also due to the fact that, in this way, the distance between test and previous $\mathbf{q}$ points is maximal and thus the largest discrepancies between the grids can be obtained. Furthermore, the already calculated dynamical matrices can be used later in the interpolation. Since the final goal is, e.g., a converged phonon dispersion curve, it makes further sense to look at the differences along some high-symmetry directions. Therefore, one inspects the differences

$$\Delta\omega = |\omega_{nnn}^{\mathrm{int}}(\mathbf{q}) - \omega_{lll}^{\mathrm{DFPT}}(\mathbf{q})|, \tag{7}$$

where $\omega_{nnn}^{\mathrm{int}}(\mathbf{q})$ is the frequency interpolated on a $n \times n \times n$ grid at a point $\mathbf{q}$ of the $l \times l \times l$ grid (for, e.g., $l=2n$), and $\omega_{lll}^{\mathrm{DFPT}}(\mathbf{q})$ is the DFPT calculated frequency at the point $\mathbf{q}$ of the $l \times l \times l$ grid. The final extent of the mini-BZ depends on the discrepancies which shall be resolved.

Since often, the phonon dispersion curves are already calculated on a $4 \times 4 \times 4$ grid, which contains a $2 \times 2 \times 2$ grid, a first hint for the extent of the mini-BZ can be found by comparing these two curves, and also the number of test $\mathbf{q}$ points might be reduced. In the following, I apply the procedure for testing purposes to the two silicon structures mentioned above and describe how to choose the mini-BZ and the required $l \times l \times l$ grid.

IV. COMPUTATIONAL DETAILS

All calculations have been carried out with the QUANTUM ESPRESSO package.[10] It is based on a plane-wave pseudopotential approach to the density-functional theory.[11,12] For silicon, I have employed a norm-conserving pseudopotential generated following the scheme suggested by von Barth and Car.[13,14] The exchange-correlation energy is described within the local-density approximation.[15,16] I have used a kinetic-energy cutoff of 40 Ry and a $20 \times 20 \times 20$ Monkhorst-Pack mesh[17] together with a Methfessel-Paxton smearing[18] using a width of 0.03 Ry to describe the electronic (metallic) ground state of the systems. The phonon frequencies have been calculated using the DFPT scheme[19–21] as implemented in the QUANTUM ESPRESSO package followed by a discrete Fourier transform as described in Sec. II.

Both the sh and bct structures have been investigated using a common body-centered orthorhombic (bco) cell (lattice constants $a \neq b \neq c$) with two atoms at (0, 0, 0) and at $(0, 0.5b, \Delta c)$ in the unit cell. The symmetry of bct requires $a=b$ and $\Delta=0.25$, whereas the symmetry of sh yields $b=\sqrt{3}c$ and $\Delta=0.5$. In fact, for sh, I use a biatomic supercell although the structure of the sh, phase can be described with just one atom in the sh unit cell. However, using the bco supercell for sh, I have access to soft modes especially at Γ, which are folded from the BZ boundary and which correspond to a distortion of the symmetric positions of the basis atoms resulting in a doubling of the sh monatomic supercell. For details of the choice of the cell, see Ref. 4. In this work, I have relaxed the ground-state geometry of the structure for a volume fixed to $184a_B^3$ for both sh and bct. The equilibrium lattice constants are $c/a=0.5489$ for bct and $c/a=0.5338$ and $b/a=0.9230$ for sh. The error with respect to the ideal b/c ratio of sh is negligible.

V. RESULTS

As a test system, I have chosen high-pressure phases of bulk silicon. The cubic-diamond structure, which is stable at normal conditions, transforms experimentally to the bct structure of the β-tin phase at around 103 kbar. The following phase transition to the *Imma* phase occurs at around 130 kbar. The *Imma* phase transforms to the simple-hexagonal phase at around 150 kbar.[22] At higher pressures, also other phases have been detected. All high-pressure phases of bulk silicon are metallic. In previous calculations,[4] I found that the β-tin phase is stable up to 115 kbar (corresponding to a volume $V=186a_B^3$), the *Imma* phase between 121 and 140 kbar $[V=(185-181)a_B^3]$, and the simple-hexagonal phase above 143 kbar (below $V=180a_B^3$), which is in agreement with the experimental finding.

For the application of the method, I have chosen the bct and the sh structures of silicon beyond the stability range of the corresponding phases, since a phonon softening had been found. Furthermore, I have chosen the same volume ($V=184a_B^3$) for both structures in order to avoid an influence of convergence parameters (i.e., the number of plane waves) on the calculation.

As the first example, I have chosen the bct structure of silicon at a pressure above the stability range of the corresponding β-tin phase. For this structure, I have found a phonon instability along the Γ-X direction of the bct BZ[23,24] which is equivalent to the Γ-T direction of the bco BZ (see Ref. 4). This phonon instability turned out not to be physical. The phonons in the mentioned articles had been calculated using a $4 \times 4 \times 4$ Monkhorst-Pack mesh, which was slightly insufficient to describe the frequencies in this region of the BZ properly, since calculations within DFPT of dynamical matrices at $\mathbf{q}$ points near Γ have yielded only real frequencies. Because the phase space of the numerically soft modes was negligibly small, the imaginary frequencies did not affect the results for the free energy. However, I use this case to check the validity of the method described in Sec. II by the use of the mini-BZ based on a $4 \times 4 \times 4$ grid outside and an $8 \times 8 \times 8$ one inside the mini-BZ. A comparison of the phonon dispersion curve using the $4 \times 4 \times 4$ grid plus the mini-BZ with to the one based on $8 \times 8 \times 8$ mesh gives an estimate of the errors using the scheme. The bct structure is also taken to exemplify the choice of the extent of the mini-BZ. Afterwards, I apply the scheme to go beyond the $8 \times 8 \times 8$ mesh.

As a second example, I have chosen the sh structure of silicon at a pressure below the stability range of the corresponding phase, here the sh phase. Choosing a biatomic supercell, a soft phonon mode has been found at the Γ and the S point of the bco BZ.[4] The imaginary frequencies at both points correspond to an instability at the L of the monatomic sh unit cell. The finding of a soft phonon mode at a zone-boundary point is in accordance with other reported results.[25–28] In fact, the softening at the BZ-boundary point L

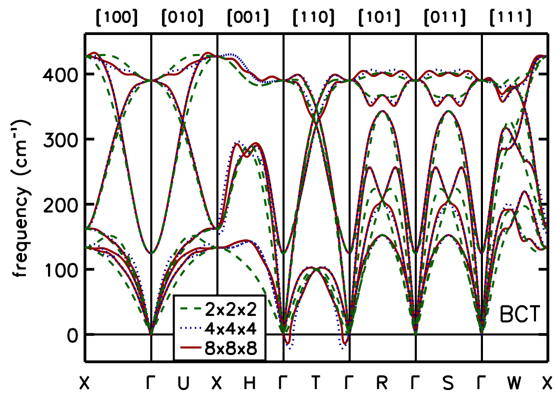

FIG. 1. (Color online) Phonon dispersion curves for the bct structure at $V=184a_B^3$. Dispersion curves obtained by Fourier transform using a $2\times2\times2$ mesh (dashed lines), a $4\times4\times4$ mesh (dotted lines), and an $8\times8\times8$ mesh (solid lines).

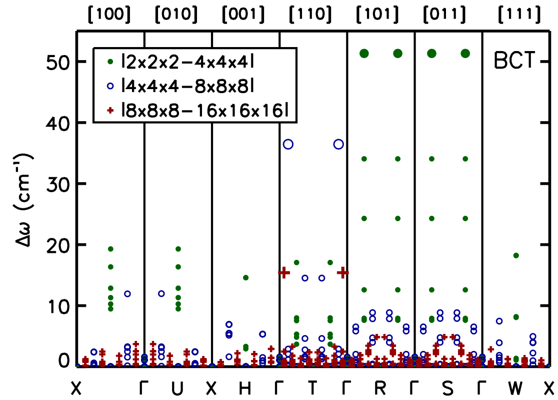

FIG. 2. (Color online) Differences $\Delta\omega$ between the calculated and Fourier-interpolated points along the high-symmetry directions for various meshes: $\Delta\omega=|\omega_{222}^{\mathrm{int}}-\omega_{444}^{\mathrm{DFPT}}|$ are drawn with solid symbols, $\Delta\omega=|\omega_{444}^{\mathrm{int}}-\omega_{888}^{\mathrm{DFPT}}|$ with open symbols, and $\Delta\omega=|\omega_{888}^{\mathrm{int}}-\omega_{16\ 16\ 16}^{\mathrm{DFPT}}|$ are with crosses (see text). Large symbols indicate the largest differences in each set.

refers to a doubling of the sh unit cell. This is in agreement with the distortion of the biatomic supercell which contains two monatomic sh cells. Thus, this soft phonon mode is of physical origin.

Both case studies—the one with an unphysical but numerically imaginary frequencies and the one with the physically correct phonon instability—are described in the following.

A. Application to the body-centered tetragonal structure of silicon

1. Standard procedure: Increasing mesh size

For the bct structure at $V=184a_B^3$ corresponding to a pressure of 133 kbar, the frequencies along the high-symmetry directions of the bco BZ have been calculated using a $2\times2\times2$, a $4\times4\times4$, and an $8\times8\times8$ grid. The results are shown in Fig. 1. Since the bct structure has a higher symmetry than the bco structure, the Γ-*X* and the Γ-*R* directions (bco) are equivalent to the Γ-*U*-*X* and the Γ-*S* directions (bct), respectively. The equivalent directions are shown mainly for completeness. The Γ-*T* direction with $T(\frac{1}{2},\frac{1}{2},0)$ (coordinates in units of reciprocal lattice vectors; in the following, I will assume the points in the BZ always in units of reciprocal lattice vectors without mentioning it explicitly) is of particular interest because a soft phonon mode appears close to Γ using the $4\times4\times4$ mesh, as visible in Fig. 1. Note that this softening does not appear for the $2\times2\times2$ grid, which is obviously insufficient to describe the phonon dispersion correctly. Increasing the mesh size, the softening remains for an $8\times8\times8$ grid, albeit, to a lesser extent. From the dispersion curves it is difficult to decide whether convergence with respect to **q** has been achieved for the $4\times4\times4$ or not, since the frequencies at the mesh points of the $8\times8\times8$ grid are on top of the Fourier-interpolated $4\times4\times4$ dispersion curves. Only for the low-frequency mode along the Γ-*T* direction are some of the interpolated frequencies imaginary, but the DFPT calculated frequencies at the $8\times8\times8$ points (not shown in the figure) are all real. Besides, the shape of the $8\times8\times8$ Fourier-interpolated phonon curves shows only minor deviations from the $4\times4\times4$ ones. Inspecting the frequencies at mesh points of the $16\times16\times16$ grid, the calculated frequencies are nearly indistinguishable from the interpolated dispersion curves except along the critical Γ-*T* direction where all calculated points yield real frequencies, while a part of the $8\times8\times8$ Fourier-interpolated phonon dispersion is imaginary.

However, such a detailed study is not always possible for every system. In this case, the $2\times2\times2$ mesh required the calculation of dynamical matrices at 4 **q** points in the IBZ, the $4\times4\times4$ mesh at 13 **q** points, and the $8\times8\times8$ mesh at 59 **q** points. Since the dispersion curves do not change significantly when assuming a grid denser than the $4\times4\times4$ (except along the Γ-*T* direction and there only in the region close to Γ), it is not necessary to calculate all the dynamical matrices on an $8\times8\times8$ or a $16\times16\times16$ grid. Ultimately, the unphysical instability should be lifted. This can be achieved by applying the method described in Sec. II using a mini-BZ around Γ. For its extent, the differences $\Delta\omega$ between the frequencies derived from the DFPT dynamical matrices and the Fourier-interpolated ones [see Eq. (7)] are analyzed. They are drawn for various **q** points along the high-symmetry directions in Fig. 2. As mentioned above, the differences $\Delta\omega$ for the $2\times2\times2$ and the $4\times4\times4$ meshes are quite large. All differences decrease significantly using a finer grid, except for the points near Γ along the Γ-*T* direction. Thus, the application of the method for a mini-BZ around Γ promises an improvement of the results especially in the range of Γ-*T*.

2. Test of the present mini-Brillouin zone method

For a first test, I want to apply the method using a $4\times4\times4$ grid outside the mini-BZ and an $8\times8\times8$ inside. The scope of this test is to reproduce the $8\times8\times8$ curves (including the numerically instable mode) using a $4\times4\times4$ mesh together with a mini-BZ, since a phonon dispersion curve using a full $8\times8\times8$ grid exists as a reference.

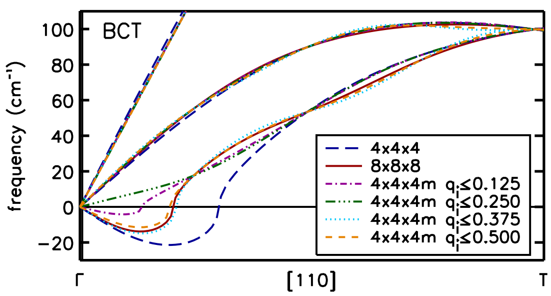

FIG. 3. (Color online) Phonon dispersion curves along Γ-T using a $4\times4\times4$ and an $8\times8\times8$ mesh together with interpolated curves ($4\times4\times4m$) based on various mini-BZs as denoted in the legend. Imaginary frequencies are drawn along the negative frequency axis. The cutoff for the **q** points is in units of reciprocal lattice vectors for q_i, with $i=x,y,z$ (see text).

Inspecting Fig. 2, the largest deviation of the $8\times8\times8$ mesh from the $4\times4\times4$ mesh (open symbols in Fig. 2) of $\Delta\omega\approx36$ cm^{-1} is found for the point $\left(\frac{1}{8},\frac{1}{8},0\right)$ along Γ-T (large symbols in Fig. 2), but also for the point $\left(\frac{3}{8},\frac{3}{8},0\right)$, the differences between the meshes are in the order of $\Delta\omega\approx15$ cm^{-1}. Besides, along X-Γ-U-X, the differences are also remarkable for **q** points with components $q_i\leq\frac{1}{4}$ ($i=x,y,z$). Thus, the selection of **q** points up to $q_i\leq\frac{3}{8}$ would be a promising choice for the mini-BZ.

In the following, I have used various mini-BZs up to $q_i\leq\frac{1}{2}$ ($i=x,y,z$) for the interpolation (denoted as $4\times4\times4m$). The results for the low-frequency range of the phonon dispersion curve along the Γ-T direction are shown in Fig. 3 in comparison with the results based on $4\times4\times4$ and $8\times8\times8$ grids. Note that the choice of $q_i\leq1$ would make the $4\times4\times4m$ grid identical to the $8\times8\times8$ grid. The curves for the mini-BZ with both $q_i\leq\frac{3}{8}$ and $q_i\leq\frac{1}{2}$ are very close to the curve using the full $8\times8\times8$ mesh. Therefore, the choice of $q_i\leq\frac{3}{8}$ for the mini-BZ, which has been already assumed from Fig. 2, is confirmed. Also, the high-frequency region of the dispersion using an $8\times8\times8$ grid is reproduced very well with this $4\times4\times4m$ grid (see Fig. 4). Only minor deviations appear at regions more distant from Γ resulting from the unresolved $\Delta\omega=6.93$ cm^{-1} along X-H-Γ. However, the general improvement of the accuracy of the phonon dispersion curve also outside the mini-BZ is remarkable. Note that with this mini-BZ, only 15 **q** points of the $8\times8\times8$ have been necessary in addition to the 13 **q** points of the $4\times4\times4$ mesh, which are much less than the 59 **q** points of the full $8\times8\times8$ grid.

3. Application of the mini-Brillouin zone to denser grids

After verifying the validity of the method, I want to go beyond the $8\times8\times8$ mesh because of the remaining unphysical softening along Γ-T. The calculated frequencies at $16\times16\times16$ mesh points along the high-symmetry directions show only real values. Inspecting the differences $\Delta\omega$ in Fig. 2 again, there is just a major difference of ≈15 cm^{-1} along Γ-T for $\mathbf{q}=\left(\frac{1}{16},\frac{1}{16},0\right)$, whereas the other differences are tiny. Since along the Γ-T direction at $\mathbf{q}=\left(\frac{3}{16},\frac{3}{16},0\right)$ there is a crucial difference of 3.3 cm^{-1}, which might be important for resolving the numerical soft mode, I have tested mini-BZs with **q** points up to $q_i\leq\frac{1}{4}$ yielding additional 29 **q** points. The results are denoted as $8\times8\times8m$. With this mini-BZ, the phonon frequencies are described accurately, as shown in Fig. 4, and the softening along Γ-T has been lifted. The curves for $8\times8\times8m$ and $4\times4\times4m$ match nearly exactly, indicating that convergence has been achieved. Note that in this case, the mini-BZ using $16\times16\times16$ points is applied in addition to the mini-BZ using $8\times8\times8$ points and in addition to the $4\times4\times4$ mesh. In fact, I achieve convergence for $8\times8\times8m$ since the remaining differences $\Delta\omega$ are less than 1.25 cm^{-1}. It has to be mentioned that further improvement could be achieved using a mini-BZ close to the points T, R, and S, which is also possible within the scheme.

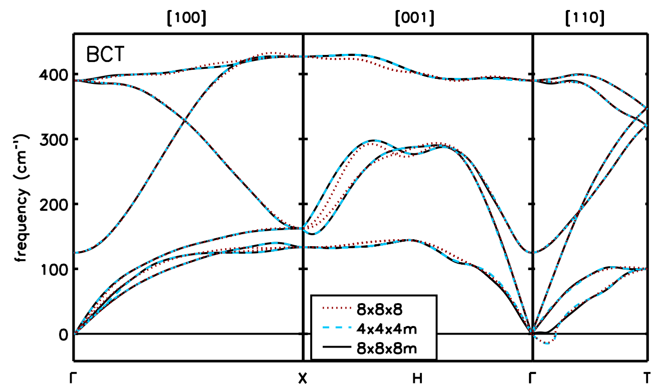

FIG. 4. (Color online) Comparison of the dispersion curves obtained from an $8\times8\times8$ grid (dotted line) using the $q_i\leq0.375$ mini-BZ in addition to the $4\times4\times4$ grid ($4\times4\times4m$, dashed line) and using $16\times16\times16$ points in the $q_i\leq0.25$ mini-BZ based on force constants from the $4\times4\times4m$ grid ($8\times8\times8m$, solid line) (see text). Imaginary frequencies are drawn along the negative frequency axis.

In summary, I have been able to obtain converged phonon dispersion curves using the total of 57 **q** points in the IBZ which is around one-sixth of the 349 **q** points that are required for a complete $16\times16\times16$ mesh. In this way, the convergence is accelerated significantly.

B. Application to the simple hexagonal structure of silicon

Similarly to bct, I have investigated the sh structure of bulk silicon at a volume $V=184a_B^3$ which corresponds here to a pressure of 107 kbar, again beyond the range of stability of the corresponding sh phase.

1. Standard procedure: Increasing mesh size

First, I compare the phonon dispersion curves using the $2\times2\times2$, the $4\times4\times4$, and the $8\times8\times8$ grids and the differences $\Delta\omega$ [see Eq. (7)] in Fig. 5. Because of the lower symmetry of the sh structure, more **q** points for each considered grid had to be calculated within DFPT: 5 points for $2\times2\times2$, 18 for $4\times4\times4$, 95 for $8\times8\times8$, and 621 for $16\times16\times16$. Inspecting Fig. 5, there are remarkable differences visible in the results based on a $2\times2\times2$ and a 4×4

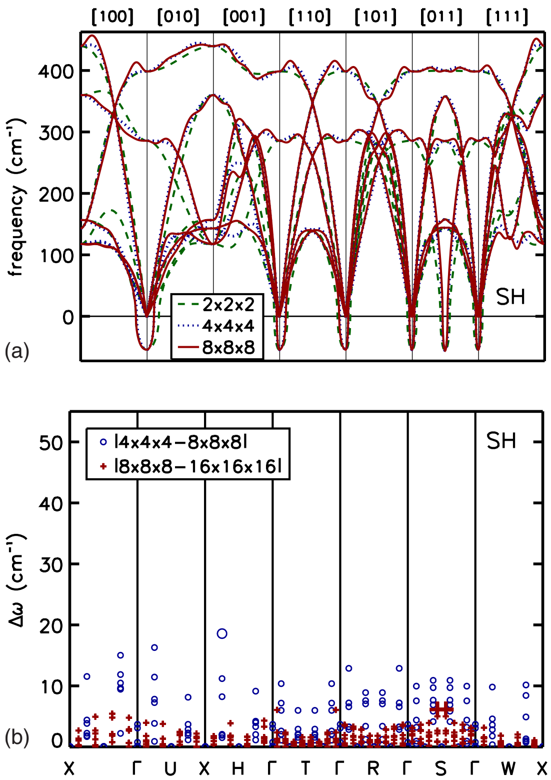

FIG. 5. (Color online) Phonon dispersion curves for the sh structure at $V=184a_B^3$. Upper panel: curves obtained from a $2\times2\times2$ mesh (dashed lines), a $4\times4\times4$ mesh (dotted lines), and an $8\times8\times8$ mesh (solid lines). Imaginary frequencies are drawn along the negative frequency axis. Lower panel: differences $\Delta\omega$ for sh as in Fig. 2 but for $\Delta\omega=|\omega_{444}^{\mathrm{int}}-\omega_{888}^{\mathrm{DFPT}}|$ and $\Delta\omega=|\omega_{888}^{\mathrm{int}}-\omega_{161616}^{\mathrm{DFPT}}|$ only.

$\times4$ mesh and between the ones based on a $4\times4\times4$ and on an $8\times8\times8$ mesh. This is reproduced in the graph of $\Delta\omega$. However, the variations along the Γ-T direction are rather small and the imaginary frequencies nearly do not change their extent in $|\mathbf{q}|$. In addition to the Γ point, there are significant differences around the X and the S points. Since the soft modes at the Γ point and the S point are in this case equivalent, an improvement at Γ will yield an improvement at S. Now, I focus on the area around the Γ point.

2. *Second test of the present method*

Looking at the differences $\Delta\omega$ between the $4\times4\times4$ and the $8\times8\times8$ meshes, the choice of $q_i\leqslant\frac{3}{8}$ as for bct is not reasonable for sh since the deviation of $\Delta\omega\leqslant18.57$ cm^{-1} along the X-H-Γ direction at $\mathbf{q}=(0,0,\frac{7}{8})$ cannot be reduced with a mini-BZ around Γ. Nevertheless, there are differences of $\Delta\omega$ in the order of 15 cm^{-1} close to Γ at $\mathbf{q}$ with $q_i\leqslant\frac{1}{4}$ which can be resolved. However, there are also significant deviations of about 12 cm^{-1} close to the R and S points. Thus, I have chosen $q_i\leqslant\frac{1}{2}$. With this mini-BZ some further 40 dynamical matrices are necessary in addition to the 18 $\mathbf{q}$ points of the $4\times4\times4$ mesh. A comparison between the phonon dispersion curves based on the full $8\times8\times8$ mesh and the one using the mini-BZ ($4\times4\times4m$) is presented in Fig. 6. The agreement is acceptable and only the overbending

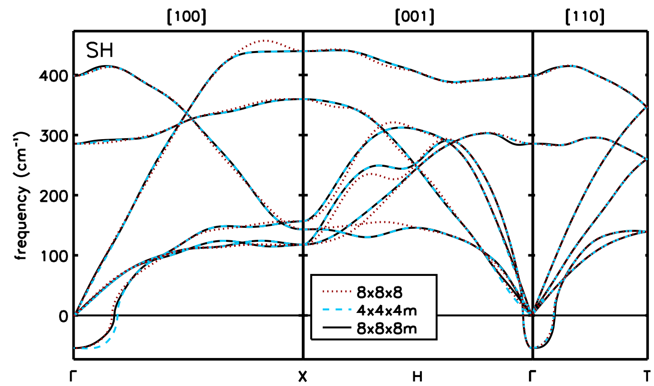

FIG. 6. (Color online) Comparison of the dispersion curves obtained from an $8\times8\times8$ grid (dotted line) using the $q_i\leqslant0.5$ mini-BZ for $8\times8\times8$ points in addition to the $4\times4\times4$ grid ($4\times4\times4m$, dashed line) and using $16\times16\times16$ points in the $q_i\leqslant0.125$ mini-BZ in addition to $4\times4\times4m$ (see text). Imaginary frequencies are drawn along the negative frequency axis.

close to the X point along [100] is not described correctly due to the choice of the mini-BZ around Γ. Using an additional mini-BZ close to X would solve this problem. However, the scope here is a check of the method for a mini-BZ around Γ analogously to the bct case (Sec. V A), and this region is described excellently.

3. *Application of the mini-Brillouin zone to go beyond the* $8\times8\times8$ *grid*

Next, I want to go beyond the $8\times8\times8$ mesh, again focusing on the region around the center of the BZ. The differences $\Delta\omega$ between the $8\times8\times8$ and the $16\times16\times16$ meshes show significant deviations for $q_i\leqslant\frac{1}{8}$, with a maximum of $\Delta\omega\leqslant6.13$ cm^{-1} at the S point, also for the Γ-X direction along [100]. In order to reduce these discrepancies and for describing especially the range of the phonon softening correctly, I have chosen $q_i\leqslant\frac{1}{8}$ for the mini-BZ by including an additional ten dynamical matrices for the calculation of the force constants. In this way, the differences 6.05 cm^{-1} are eliminated along Γ-T. The resulting phonon dispersion curve is presented in Fig. 6. One can notice the improvement of the results based on the $4\times4\times4m$ and the $8\times8\times8m$ grids.

Regarding the numerical effort, I have used 18 dynamical matrices of the $4\times4\times4$ mesh, an additional 40 of the $8\times8\times8$ one, and a furthermore 10 of the $16\times16\times16$ grid, giving 68 in total. This is much less than the 621 dynamical matrices required for a complete $16\times16\times16$ grid. Also, in this case, the numerical effort has been reduced drastically.

C. Discussion

For both systems, the bct and the sh structures of bulk silicon, I have been able to apply the scheme successfully and I have obtained converged phonon dispersion curves using less $\mathbf{q}$ points than needed for the corresponding full mesh. On comparing the results of the bct and the sh structures, one can see that the convergence of the sh structure with respect to the **q** points is slower than that of the bct structure which results in a larger choice of the mini-BZ. In particular, for bct, the critical region with large variations with respect to the choice of the **q** mesh is around the center of the BZ, whereas for sh, it is around X. Since the ground state of both structures had been calculated using the same convergence parameters and the same unit cell at the same volume, the different speed of the **q** convergence is not due to different convergence parameters for the ground state. Therefore, one cannot estimate the size of the **q**-point grid which is required for convergence from one structure to another, even using the same cell. Thus, the **q**-point convergence has to be tested for any structure separately. It was possible, however, to confirm the soft phonon mode at Γ for the sh structure, whereas the one of the bct structure has disappeared including enough **q** points around the center of the BZ. Hence, the latter suspected phonon instability is due to an inaccurate description of the long-range force constants, and thus, it has only numerical origin. It would be possible to reduce the remaining discrepancies for sh around the X point (overbending) using the method by applying an additional mini-BZ. This is beyond the scope of this paper, however.

VI. CONCLUSIONS

I have presented a scheme within standard DFPT calculations for the accurate calculation of phonon dispersion curves by improving the interatomic force constants which can be applied for semiconducting systems as well as for metallic ones. The long-range contribution to the force constants, in particular, can be described successfully. This scheme is based on the inclusion of a denser **q**-point mesh in some part of the BZ (mini-BZ) and a wider one outside. The method has been applied successfully to the bct and the sh structures of bulk silicon, where the origin of the phonon instabilities has been discussed. In detail, for the bct structure, the soft phonon mode has been traced back to an inaccurate description of the (long-range) force constants, and the imaginary frequencies become real after applying the procedure until convergence. In the case of the sh structure, the soft phonon mode has been confirmed. For both cases, the number of required dynamical matrices has been reduced drastically. Whereas here the mini-BZ has been chosen around the center of the BZ, the scheme allows also a different choice. In this way, features at the boundary of the BZ can also be described more accurately. Another application of this technique could be the mixing of force constants based on different grids, e.g., $3\times3\times3$ and $4\times4\times4$ meshes. The range of the force constants is doubled when moving from a $n\times n\times n$ grid to a $2n\times2n\times2n$. Nothing can be said about the range of the resulting mixed force constants in the case of the mixing of incommensurate grids. In summary, the use of the method can improve results not only for phonon dispersion curves but also for related quantities such as Grüneisen parameters, thermal expansion, and the free energy.

ACKNOWLEDGMENTS

Support by the Heinrich Böll Stiftung, Germany, is gratefully acknowledged. Computer facilities at CINECA granted by INFM (Project No. 643/2006) are gratefully acknowledged. This work was funded in part by the EU's 6th Framework Programme through the NANOQUANTA Network of Excellence (NMP-4-CT-2004-500198). I want to thank in particular Dieter Strauch for many fruitful discussions. Without his ideas, this project would not have been possible. I also want to thank Conor Hogan for helpful discussions and for correcting the paper.

*katalin.gaal-nagy@physik.uni-regensburg.de

[1] L. J. Zhang, Y. L. Niu, T. Cui, Y. Li, Y. Wang, Y. M. Ma, Z. He, and G. T. Zou, J. Phys.: Condens. Matter **18**, 9917 (2006).
[2] Y. Li, L. Zhang, T. Cui, Y. Ma, G. Zou, and D. D. Klug, Phys. Rev. B **74**, 054102 (2006).
[3] H. R. Xia, S. Q. Sun, X. F. Cheng, S. M. Dong, H. Y. Xu, L. Gao, and D. L. Cui, J. Appl. Phys. **98**, 033513 (2005).
[4] K. Gaál-Nagy and D. Strauch, Phys. Rev. B **73**, 014117 (2006).
[5] J. Han, F. Wan, Z. Zhu, and W. Zhang, Appl. Phys. Lett. **90**, 031104 (2007).
[6] S. Baroni, S. de Gironcoli, A. D. Corso, and P. Giannozzi, Rev. Mod. Phys. **73**, 515 (2001).
[7] J. Ihm, M. T. Yin, and M. L. Cohen, Solid State Commun. **37**, 491 (1981).
[8] N. W. Ashcroft and N. D. Mermin, *Solid State Physics* (Saunders, Fort Worth, 1976).
[9] X. Gonze and C. Lee, Phys. Rev. B **55**, 10355 (1997).
[10] http://www.pwscf.org.
[11] P. Hohenberg and W. Kohn, Phys. Rev. **136**, B864 (1964).
[12] W. Kohn and L. J. Sham, Phys. Rev. **140**, A1133 (1965).
[13] U. von Barth and R. Car (unpublished).
[14] A. DalCorso, S. Baroni, R. Resta, and S. de Gironcoli, Phys. Rev. B **47**, 3588 (1993).
[15] J. P. Perdew and A. Zunger, Phys. Rev. B **23**, 5048 (1981).
[16] D. M. Ceperley and B. J. Alder, Phys. Rev. Lett. **45**, 566 (1980).
[17] H. J. Monkhorst and J. D. Pack, Phys. Rev. B **13**, 5188 (1976).
[18] M. Methfessel and A. T. Paxton, Phys. Rev. B **40**, 3616 (1989).
[19] S. Baroni, P. Giannozzi, and A. Testa, Phys. Rev. Lett. **58**, 1861 (1987).
[20] P. Giannozzi, S. de Gironcoli, P. Pavone, and S. Baroni, Phys. Rev. B **43**, 7231 (1991).
[21] S. de Gironcoli, Phys. Rev. B **51**, 6773 (1995).
[22] M. I. McMahon and R. J. Nelmes, Phys. Rev. B **47**, R8337 (1993).
[23] K. Gaál-Nagy, A. Bauer, M. Schmitt, K. Karch, P. Pavone, and D. Strauch, Phys. Status Solidi B **211**, 275 (1999).
[24] K. Gaál-Nagy, M. Schmitt, P. Pavone, and D. Strauch, Comput. Mater. Sci. **22**, 49 (2001).
[25] K. J. Chang and M. L. Cohen, Phys. Rev. B **30**, R5376 (1984).
[26] R. J. Needs and R. M. Martin, Phys. Rev. B **30**, R5390 (1984).
[27] K. J. Chang and M. L. Cohen, Phys. Rev. B **31**, 7819 (1985).
[28] K. J. Chang, M. M. Dacorogna, M. L. Cohen, J. M. Mignot, G. Chouteau, and G. Martinez, Phys. Rev. Lett. **54**, 2375 (1985).